

# Noise Analysis of Conventional and Gain-Clamped Semiconductor Optical Amplifiers

Guido Giuliani, *Member, IEEE*, and Davide D'Alessandro, *Student Member, IEEE*

**Abstract**—We present a numerical study of the noise of conventional and gain-clamped semiconductor optical amplifiers (SOAs), using a detailed device model. The model makes use of a density-matrix gain calculation, and takes into account the forward and backward amplified spontaneous emission (ASE) spectra and the spatial carrier hole-burning. The device is longitudinally divided into  $M$  sections and a rate equation for averaged photon and carrier densities is used for each section. We demonstrate that the accuracy on the calculated noise figure strictly depends on the number of sections  $M$ . We obtain a good tradeoff between the results accuracy and the computational complexity with  $M = 8$ . The model is then applied to study the noise in a distributed Bragg reflector (DBR)-type gain-clamped SOA for varying signal power, pump current, and lasing wavelength. We show that changes in the spatial carrier profile caused by the input signal significantly affect the noise figure, even when the gain is constant. A slight dependence of the noise figure on lasing wavelength is also foreseen, while the dependence on the pump current is negligible. A new method for gain-clamped SOA noise figure reduction is proposed, based on unbalanced Bragg reflectors. An improvement of noise figure (NF) as large as 2 dB is devised.

**Index Terms**—Amplified spontaneous emission (ASE), optical noise, semiconductor optical amplifiers.

## I. INTRODUCTION

SEMICONDUCTOR optical amplifiers (SOAs) have been successfully demonstrated as switch matrices [1] and gate arrays [2]. These devices are likely to be used in optical cross-connects (OXC) nodes operating in wavelength-division multiplexing (WDM). The integrability of several devices on the same substrate makes them promising for the possible reduction of the functional node complexity. To overcome the limitations of conventional SOAs performances, caused by the low saturation input power in conjunction with a fast gain dynamics, gain-clamped semiconductor optical amplifiers (GC-SOAs) have been proposed and fabricated [3]. Gain clamping is achieved through laser action at an out-of-band wavelength, obtained by means of two distributed Bragg reflector (DBR) selective mirrors. GC-SOAs exhibit reduced intermodulation distortion, and can be used as low-crosstalk switches and gates in WDM applications.

The SOA noise is a crucial issue for the performance evaluation of transmission systems featuring cascaded devices. The

noise figure (NF) of conventional and wavelength-converter SOAs have been studied theoretically and experimentally in a number of papers [4], [5]. GC-SOAs have been studied with respect to crosstalk, high-input power operation, and input-signal dynamics [6]–[8], but no systematic analysis of the NF of GC-SOA has been reported.

In the present work, we study the noise of conventional SOAs and of GC-SOAs using a detailed numerical model in which the device is longitudinally divided into  $M$  sections to take into account the longitudinal spatial carrier hole-burning. Shtaif *et al.* [9] showed that the noise of SOAs is made of both the conventional broadband ASE noise and a narrow-band term arising from nonlinear carrier effects. Here, we focus on the broad-band noise, and consider saturation effects through the longitudinal carrier hole-burning.

The first result of this work is the optimization of the computational algorithm in such a way as to minimize the numerical complexity. Furthermore, we find new results on GC-SOA noise that allows a better comprehension of the physical phenomena related to the longitudinal carrier density profile along the active waveguide. We also propose a new GC-SOA configuration capable of a reduced NF.

The paper is organized as follows. Section II describes the device model. In Section III, we reformulate the calculation of the SOA NF and investigate the tradeoff between the accuracy of the calculated NF and the computational complexity. We find that the optimum number of sections into which the device must be divided is  $M = 8$ . In Section IV, we perform a systematic analysis of the NF for GC-SOAs. The NF is studied as a function of input signal power, pump current, lasing wavelength, and Bragg reflectivities. We demonstrate that the NF is affected to a large extent by the longitudinal carrier profile, and that it varies with the input signal power, even when the gain is constant. Furthermore, our analysis shows that the NF slightly depends on the lasing wavelength, while its dependence on the pump current is negligible. Finally, in Section V, a new GC-SOA configuration is proposed to improve the noise and crosstalk performance. We foresee that a device with unbalanced Bragg reflectors can achieve up to 2-dB NF reduction without affecting either the gain or the saturation characteristics.

## II. SOA MODEL

A reliable evaluation of SOA performances requires correct descriptions for the material gain and carrier recombinations. In particular, the radiative recombination stimulated by signal and ASE photons is essential. The present model uses a density-matrix approach for material gain calculation, and takes the effective ASE spectrum and the longitudinal carrier nonuniformity

Manuscript received July 30, 1999 revised June 13, 2000. This work was performed under a CNR-MADESS II Contract.

The authors are with Dipartimento di Elettronica, Università di Pavia, I-27100 Pavia, Italy (e-mail: giuliani@ele.unipv.it).

Publisher Item Identifier S 0733-8724(00)08078-6.

TABLE I  
LIST OF PARAMETER VALUES

Symbol	Meaning	Value
$\Gamma$	mode confinement factor	0.7
$\alpha$	waveguide loss	$70 \text{ cm}^{-1}$
$\tau_{\text{in}}$	intradband relaxation time	$10^{-13} \text{ s}$
$\beta_{\text{las}}$	lasing mode spontaneous coupling factor	$10^{-4}$
$\lambda_{\text{las}}$	lasing wavelength	1520 nm (default)
$\lambda_{\text{sig}}$	signal wavelength	1550 nm
$A$	defect recombination coefficient	$2.8 \cdot 10^8 \text{ s}^{-1}$
$B$	radiative recombination coefficient	$4.26 \cdot 10^{-11} \text{ cm}^3 \cdot \text{s}^{-1}$
$C$	Auger recombination coefficient	$6.5 \cdot 10^{-29} \text{ cm}^6 \cdot \text{s}^{-1}$
$d$	active region thickness	$0.16 \text{ }\mu\text{m}$
$L$	SOA length	$400 \text{ }\mu\text{m}$
$R_1$	input end Bragg grating reflectivity	0.03 (default)
$R_2$	output end Bragg grating reflectivity	0.03 (default)
$v_g$	group velocity	$8.57 \cdot 10^9 \text{ cm} \cdot \text{s}^{-1}$
$w$	active region width	$2 \text{ }\mu\text{m}$

into account. A  $1.55\text{-}\mu\text{m}$  bulk InGaAsP active material SOA is considered. A list of SOA parameters is reported in Table I.

In the following, we discuss the main issues on which our SOA model is based.

#### A. Gain Model

The material gain is a function of the wavelength  $\lambda$  and of the injected carrier density  $N$  and it is defined as

$$g_{\text{mat}}(N, \lambda) = E_{\text{st}}(N, \lambda) - E_a(N, \lambda) \quad (1)$$

where  $E_{\text{st}}(N, \lambda)$  and  $E_a(N, \lambda)$  are, respectively, the rates per unit length of stimulated emission and absorption, and are calculated using the density-matrix approach [10]. The calculation takes into account light- and heavy-hole band transitions, energy-gap dependence on carrier density, and intraband relaxation time  $\tau_{\text{in}}$ . The quasi-Fermi levels are evaluated according to the Joyce–Dixon approximation [10], while the intraband relaxation time is accounted for by convolution in the frequency domain with a Lorentzian line shape with full-width at half-maximum (FWHM) =  $1/(\pi\tau_{\text{in}})$  [11].

#### B. Amplified Spontaneous Emission

The coefficient of spectral spontaneous photon density generation rate  $\rho_{\text{sp}}(N, \lambda)$  is calculated from  $E_{\text{st}}(N, \lambda)$  using the Einstein relations [12]. The spontaneous coupling coefficient  $\beta(\lambda)$  represents the fraction of spontaneously emitted photons that couple into the guided mode. It is given by [13]

$$\beta(\lambda) = \frac{\lambda^2 \Gamma}{8\pi n_{\text{eff}}^2 w d} \quad (2)$$

where  $\Gamma$  is the mode confinement factor, and  $n_{\text{eff}}$  is the mode effective index. The value of  $\beta(\lambda)$  ranges from  $1.5 \times 10^{-2}$  at 1450 nm to  $1.94 \times 10^{-2}$  at 1650 nm. In the calculations, the ASE spectrum is divided into ten, 20-nm-wide, spectral slices. The accurate description of the spontaneous emission is essential to reveal gain saturation effects caused by ASE, that are relevant for small-signal intensity and/or high current injection.

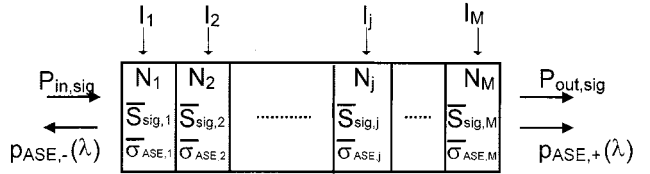


Fig. 1. The SOA is longitudinally divided into  $M$  sections of equal length.  $P_{\text{in}}$  and  $P_{\text{out}}$  are input and output signal power,  $p_{\text{ASE},+}$  and  $p_{\text{ASE},-}$  are co- and counterpropagating ASE spectral densities.  $\bar{S}_{\text{sig},j}$  and  $\bar{\sigma}_{\text{ASE},j}$  are, respectively, the spatially averaged signal and ASE photon densities in section  $j$ .

#### C. SOA Sectioning

In a simplified SOA model, a single rate-equation for spatially averaged values of carrier and photon density can be used [14]. Such a model can be helpful for the coarse definition of device fabrication parameters, but does not allow to accurately determine its performances.

A more detailed model must take into account the longitudinal spatial nonuniformity of the carrier density, which is a consequence of the almost exponential spatial profile of signal and ASE powers within the SOA. In our model, the SOA is divided into  $M$  longitudinal sections of equal length, and a simplified model with uniform carrier and averaged photon densities is used for each section. Terminal facet reflectivity is neglected, since reflectivities smaller than  $10^{-4}$  have been obtained in reported devices [2].

Fig. 1 illustrates the SOA sectioning. The  $j$ th section has a uniform carrier density  $N_j$ , an averaged signal photon density  $\bar{S}_{\text{sig},j}$ , and an averaged ASE spectral photon density  $\bar{\sigma}_{\text{ASE},j}$ . The total current injected into the active region  $I_{\text{act}}$  is supposed to be equally distributed among the sections, hence  $I_j = I_{\text{act}}/M$ . Current leakage effects are neglected: thus for a real device, the gain values calculated here will be obtained at higher total injected currents.

In stationary conditions (i.e.,  $dN/dt = 0$ ), the following rate equation holds for each section:

$$\frac{I_j}{qwdL_j} = R_{\text{sp},j}(N_j) + R_{\text{stim, sig},j}(\mathbf{N}, S_{\text{in, sig}}, \lambda_{\text{sig}}) + R_{\text{stim, ASE},j}(\mathbf{N}), \quad j = 1, 2, \dots, M \quad (3)$$

where  $L_j$  is the length of the  $j$ th section,  $\mathbf{N} = (N_1, N_2, \dots, N_M)$  is the vector of sections carrier densities,  $S_{\text{in, sig}}$  is the input signal photon density, and  $\lambda_{\text{sig}}$  is the signal wavelength. The spontaneous recombination term is given by

$$R_{\text{sp},j}(N_j) = AN_j + BN_j^2 + CN_j^3$$

where the first term accounts for defects recombination, the second for spontaneous radiative recombination, and the third for Auger recombination. The spontaneous recombination  $R_{\text{sp},j}(N_j)$  only depends on the average carrier density of the  $j$ th section  $N_j$ , while the stimulated recombination terms due to signal and ASE photons also depend on the carrier density of other sections.

The signal-stimulated recombination is calculated by averaging the signal photon density in the  $j$ th section [14]

$$R_{\text{stim, sig},j}(\mathbf{N}, S_{\text{in, sig}}, \lambda_{\text{sig}}) = v_g g_{\text{mat}}(N_j, \lambda_{\text{sig}}) \frac{G(N_j, \lambda_{\text{sig}}) - 1}{\ln G(N_j, \lambda_{\text{sig}})} S_{\text{in, sig},j} \quad (4)$$

where  $v_g$  is group velocity and

$$G(N_j, \lambda_{\text{sig}}) = \exp[\Gamma \cdot g_{\text{mat}}(N_j, \lambda_{\text{sig}}) - \alpha] \cdot L_j$$

is the gain of the  $j$ th section, with  $\alpha$  as the waveguide-loss coefficient. The  $j$ th-section input photon density  $S_{\text{in, sig},j}$  is calculated as the SOA input photon density  $S_{\text{in, sig}}$  multiplied by the gain of preceding sections.

The ASE stimulated recombination is given by

$$\begin{aligned} R_{\text{stim, ASE},j}(\mathbf{N}) &= v_g \int g_{\text{mat}}(N_j, \lambda) \\ &\quad \cdot [\bar{\sigma}_{\text{sp},j}(N_j, \lambda) + \bar{\sigma}_{\text{ASE, in},j}(\mathbf{N}, \lambda)] d\lambda \\ &= v_g \int g_{\text{mat}}(N_j, \lambda) \\ &\quad \cdot \left[ \frac{2\Gamma\beta(\lambda)\rho_{\text{sp}}(N_j, \lambda)}{v_g(\Gamma g_{\text{mat}}(N_j, \lambda) - \alpha)} \left( \frac{G(N_j, \lambda) - 1}{\ln G(N_j, \lambda)} - 1 \right) \right. \\ &\quad \left. + \frac{G(N_j, \lambda) - 1}{\ln G(N_j, \lambda)} \bar{\sigma}_{\text{ASE, in},j}(\mathbf{N}, \lambda) \right] d\lambda \quad (5) \end{aligned}$$

and it depends on both the spatially averaged spectral density of spontaneous photons generated within the  $j$ th section ( $\bar{\sigma}_{\text{sp},j}(N_j, \lambda)$ ) and on the spatially averaged spectral density of ASE photons, generated in all other sections, that enter the  $j$ th section from both sides ( $\bar{\sigma}_{\text{ASE, in},j}(\mathbf{N}, \lambda)$ ). For the

numerical calculation, the integral in (5) is replaced by a finite sum over the ten spectral slices into which the ASE spectrum is divided.

Equation (3) represents a set of  $M$  mutually coupled nonlinear equations with unknown  $\mathbf{N}$ . This set is numerically solved using a gradient least squares method, letting the pump current and the input signal power and wavelength be the varying parameters. Obviously, an increase in  $M$  gives more accurate results, at the cost of increased computational time. Once the longitudinal carrier density distribution  $\mathbf{N}$  is known, the signal gain and the output ASE spectrum can be calculated.

#### D. SOA Noise Figure

The noise performance of the SOA is assessed by calculating the device NF for a coherent input signal. Physical interpretation of optical amplifier noise can be accomplished either in terms of a photon particle [15] or a wave-like description [16]. In the former case, the output noise stems from the amplifier's gain randomness, while in the latter it can be ascribed to the amplification of vacuum field fluctuations. The wave-like approach is better suited to describe noise properties of practical optical amplifiers [17]. Using the wave-like method, the NF of an optical amplifier with longitudinally nonuniform inversion can be calculated in two ways.

First, the device can be thought of as a cascade of  $M$  smaller amplifiers with uniform inversion that correspond to the  $M$  subsections, and the NF cascading formula [18] can be used. The NF of each subsection is

$$\text{NF}_{\text{sub}} \approx \frac{2N_{\text{sp, sub}}(G_{\text{sub}} - 1)}{G_{\text{sub}}} + \frac{1}{G_{\text{sub}}}$$

where  $G_{\text{sub}}$  is the gain of the subsection and  $N_{\text{sp, sub}}$  is its spontaneous emission factor [18]. The correct expression for  $N_{\text{sp}}$  in a semiconductor gain medium is

$$N_{\text{sp}}(N, \lambda) = \frac{\gamma}{\gamma - \alpha} = \frac{\Gamma E_{\text{st}}(N, \lambda)}{\Gamma E_{\text{st}}(N, \lambda) - [\Gamma E_a(N, \lambda) + \alpha]} \quad (6)$$

where  $\gamma$  is the net rate of stimulated emission and  $\alpha$  the net rate of absorption. When a phenomenological gain model is used instead of a quantum-mechanical one, the spontaneous emission factor is calculated as  $N_{\text{sp}} = N/(N - N_0)$  [19], where  $N_0$  is the carrier density at transparency. However,  $N$  and  $N_0$  are not truly proportional to the stimulated emission and absorption rates, and the use of a phenomenological gain model can cause inaccurate noise calculation.

Using the second method, the NF can be obtained by calculating the total output ASE spectrum and by applying a formula to obtain the spectrum of the photodetected current [16]. It is essential that the exact coefficient of spectral spontaneous photon density generation rate  $\rho_{\text{sp}}(N, \lambda)$  be used for each subsection, together with the appropriate spontaneous coupling coefficient  $\beta(\lambda)$ . It can be demonstrated that the two illustrated approaches give the same numerical results. In this work, we calculate the NF from the output ASE (second method). Throughout the paper, we assume that an ASE filter with 1-nm bandwidth is placed in front of the detector.

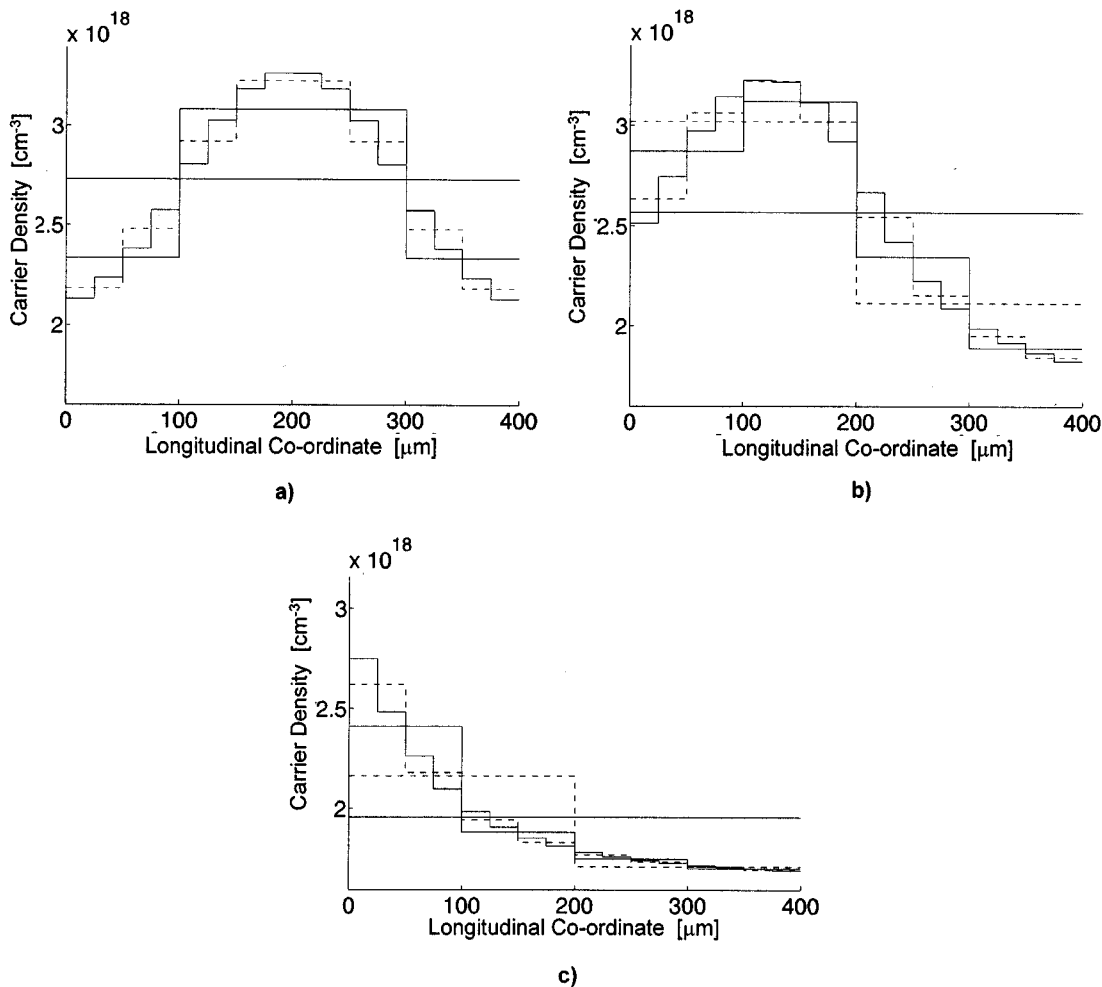


Fig. 2. Longitudinal carrier density profiles in a conventional SOA as calculated using  $M = 1, 2, 4, 8, 16$  subsections.  $I_{act} = 80$  mA,  $\lambda_{sig} = 1550$  nm. a) absence of input signal; b)  $P_{in, sig} = -20$  dBm; c)  $P_{in, sig} = 0$  dBm.

### III. RESULTS FOR CONVENTIONAL SOA

Our model converges to the exact solution when the number of sections  $M$  tends to infinity. To evaluate the optimized computational complexity of the model, we now determine the minimum required value of  $M$  to obtain accurate results for the gain and the NF. To this end, the set of equations (3) is successively solved for increasing  $M$ , i.e.,  $M = 1, 2, 4, 8, 16$ . The current injected into the active region is  $I_{act} = 80$  mA, and the calculations are performed for three significant cases, namely: a) absence of input signal; b) regime of weak saturation ( $P_{in, sig} = -20$  dBm); c) regime of strong saturation ( $P_{in, sig} = 0$  dBm). Fig. 2 reports the calculated longitudinal carrier density profiles. For case a), the carrier profile is symmetrical and is determined by the stimulated recombination due to ASE photons that deplete the input and output ends of the active waveguide. A comparison of the solutions for  $M = 1$  and  $M = 16$  shows that the difference in the calculated local carrier density can be larger than 25%. In case c), the intense input signal causes a strong saturation, and a highly asymmetric carrier profile is obtained. Fig. 2(b) reports an intermediate case in which both signal and ASE photons influence the carrier profile, that exhibits a maximum closer to the input end with respect to case a). Figs. 3 and 4

report the calculated gain and NF for  $I_{act} = 50$  mA as a function of the number of sections  $M$ . The calculation is repeated for several input powers. By increasing  $M$  from 1 to 16, the calculated gain decreases by  $1 \div 1.5$  dB for all input powers, while the NF exhibits variations of  $1.5 \div 2$  dB that are not monotonic with increasing  $M$ . At least  $M = 8$  sections are required to obtain an accuracy better than 0.1 dB for both gain and NF.

### IV. NOISE FIGURE GAIN-CLAMPED SOA

Now we apply the model described in Section II to calculate the NF of a DBR-type gain-clamped SOA. We investigate the noise performance with respect to input signal power, injected current, and lasing wavelength. In this device, laser action is achieved by means of two distributed Bragg gratings located at the input and output ends of the device. The signal gain is clamped at the value imposed by the population inversion at laser threshold, and gain saturation occurs only when the input power is large enough to turn the laser off. Thus the input signal dynamics is enhanced, and crosstalk effects are reduced [3], [6].

Two ideal reflectivities  $R_1$  and  $R_2$ , located, respectively, at the input and output waveguide ends, model the Bragg gratings. These reflectivities are centered at the lasing wavelength  $\lambda_{las}$ ,

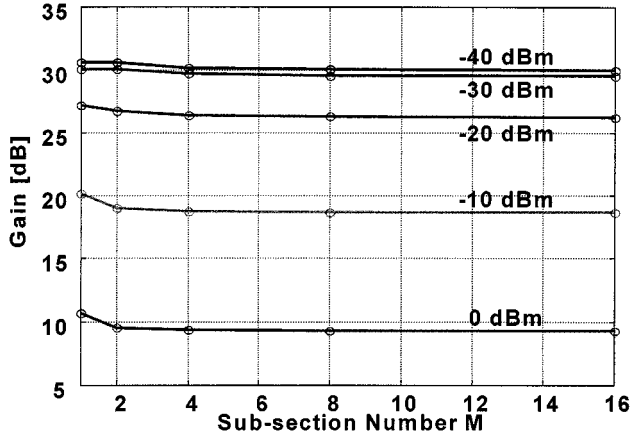


Fig. 3. Calculated signal gain for conventional SOA as a function of the number of subsections  $M$ .  $I_{\text{act}} = 50$  mA,  $\lambda_{\text{sig}} = 1550$  nm. The calculations are repeated for several input power values, reported on the graph.

and are supposed to be zero at wavelengths different from  $\lambda_{\text{las}}$ . For the GC-SOA analysis, the device is divided into  $M = 16$  sections to describe more accurately the effects of the longitudinal carrier distribution. However, we evaluate that  $M = 8$  sections would yield sufficiently accurate results also for this case.

The rate equation for the generic  $j$ th section shall be modified to take the stimulated recombination term due to lasing photons into account

$$\begin{aligned} \frac{I_j}{qwdL_j} = & R_{\text{sp},j}(N_j) + R_{\text{stim, sig},j}(\mathbf{N}, S_{\text{in, sig}}, \lambda_{\text{sig}}) \\ & + R_{\text{stim, ASE},j}(\mathbf{N}) + R_{\text{stim, las},j}(\mathbf{N}, R_1, R_2, \lambda_{\text{las}}) \end{aligned} \quad (7)$$

The new term is given by

$$\begin{aligned} R_{\text{stim, las},j}(\mathbf{N}, R_1, R_2, \lambda_{\text{las}}) = & v_g g_{\text{mat}}(N_j, \lambda_{\text{las}}) \\ & \cdot [\bar{S}_{\text{las, sp},j}(N_j, \lambda_{\text{las}}) + \bar{S}_{\text{las, in},j}(\mathbf{N}, R_1, R_2, \lambda_{\text{las}})] \\ = & v_g g_{\text{mat}}(N_j, \lambda_{\text{las}}) \\ & \cdot \left[ \frac{2\Gamma\beta_{\text{las}}\rho_{\text{sp, las}}(N_j, \lambda_{\text{las}})}{v_g(\Gamma g_{\text{mat}}(N_j, \lambda_{\text{las}}) - \alpha)} \left( \frac{G(N_j, \lambda_{\text{las}}) - 1}{\ln G(N_j, \lambda_{\text{las}})} - 1 \right) \right. \\ & \left. + \frac{G(N_j, \lambda_{\text{las}}) - 1}{\ln G(N_j, \lambda_{\text{las}})} S_{\text{las, in},j}(\mathbf{N}, R_1, R_2, \lambda_{\text{las}}) \right] \end{aligned} \quad (8)$$

where  $\beta_{\text{las}}$  accounts for the coupling of spontaneous photons into the lasing mode, and  $\rho_{\text{sp, las}}(N_j, \lambda_{\text{las}})$  is the rate of spontaneous generation.  $\bar{S}_{\text{las, sp},j}$  is the average density of lasing mode photons spontaneously generated within the  $j$ th section and  $\bar{S}_{\text{las, in},j}$  is the average density of lasing mode photons entering the  $j$ th section from both sides. The density  $S_{\text{las, in},j}(\mathbf{N}, R_1, R_2, \lambda_{\text{las}})$  of lasing-mode photons that enter the  $j$ th section depends on the spontaneous generation rate in other sections and, more heavily, on the cavity gain, which needs to be calculated for each rate equation evaluation. In a GC-SOA with low input signal power, the longitudinal carrier profile is determined mainly by the longitudinal distribution of lasing power

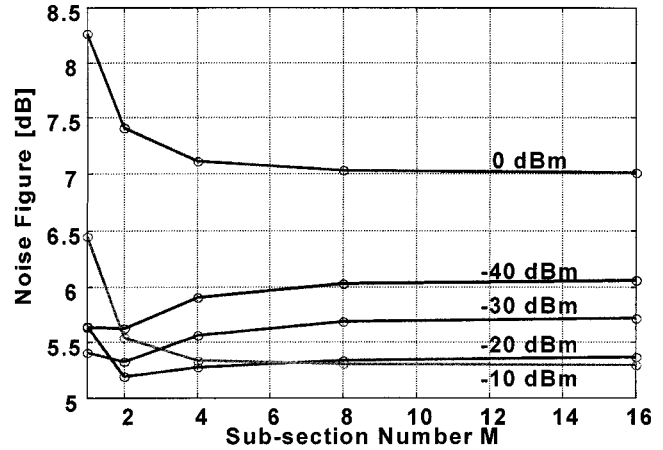


Fig. 4. Calculated noise figure for conventional SOA as a function of the number of subsections  $M$ .  $I_{\text{act}} = 50$  mA,  $\lambda_{\text{sig}} = 1550$  nm, ASE filter bandwidth = 1 nm. The calculations are repeated for several input power values, reported on the graph.

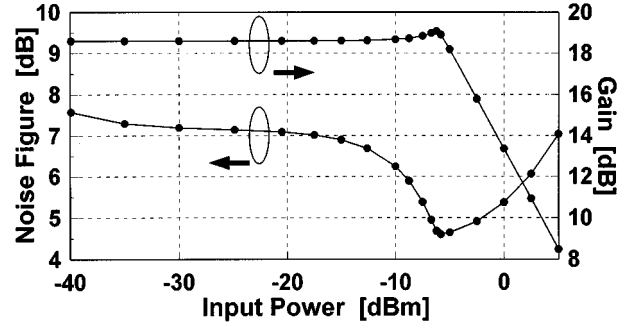


Fig. 5. Calculated gain and noise figure for a GC-SOA as a function of input signal power.  $I_{\text{act}} = 100$  mA,  $\lambda_{\text{sig}} = 1550$  nm,  $R_1 = R_2 = 0.03$ ;  $\lambda_{\text{las}} = 1520$  nm, ASE filter bandwidth = 1 nm.

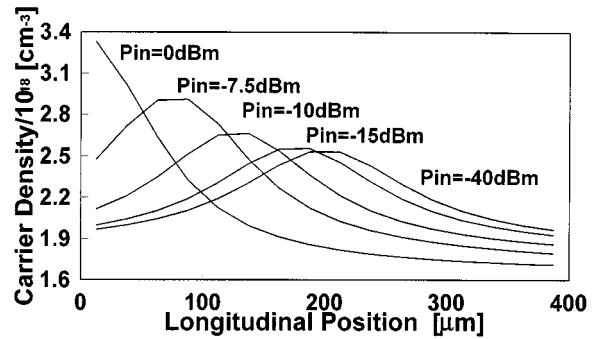


Fig. 6. Longitudinal carrier density profiles in a GC-SOA for several values of the input-signal power (reported on the graph). Parameters as in Fig. 5.

within the cavity, rather than by ASE. This happens because the lasing mode is much more intense than the ASE. The profile of lasing photons depends on the cavity losses, i.e., on the waveguide loss and on the Bragg reflectivities  $R_1$  and  $R_2$ . Thus the Bragg reflectivities influence to a large extent the longitudinal carrier-density profile.

A GC-SOA with the same length and waveguide geometry of the conventional SOA is considered. The default lasing wavelength is  $\lambda_{\text{las}} = 1520$  nm, and the Bragg reflectivities are  $R_1 =$

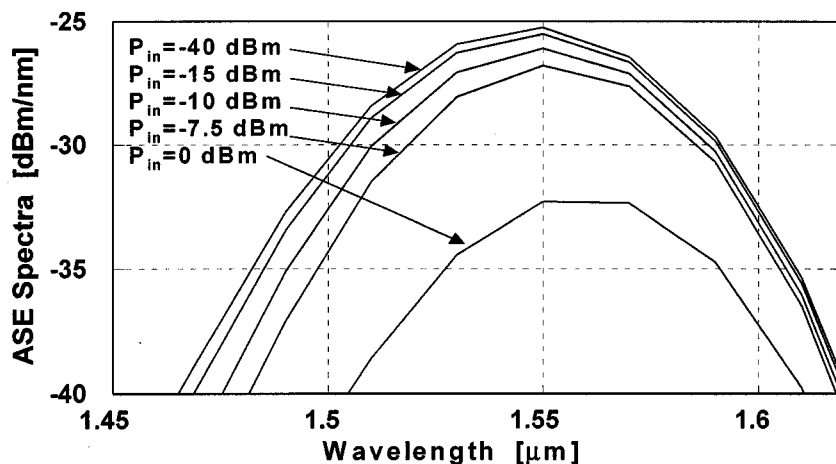


Fig. 7. Output ASE spectra of a GC-SOA for different values of the input signal power (reported on the graph). Parameters as in Fig. 5. For  $P_{in} = 0$  dBm, the gain is saturated, while for all other values the gain is clamped and, interestingly, a decrease of the ASE is observed.

$R_2 = 0.03$ . With these parameters, a threshold current of 28 mA is obtained. The GC-SOA is pumped by a 100-mA current and emits 14.5-mW laser power per facet in the absence of input signal.

Fig. 5 reports the GC-SOA gain and NF for a 1550-nm signal as a function of input power. The gain is 18.6 dB, and it remains constant up to  $-7$ -dBm input power. Beyond this value, the laser turns off and the gain saturates. The NF has a relevant decrease just before saturation occurs, and it then increases. The reason for the NF decrease can be explained by Fig. 6, that shows the longitudinal carrier-density profile for varying input power. The GC-SOA can be thought as a cascade of smaller SOAs, represented by the  $M$  subsections. In a cascade of amplifiers, the overall NF is primarily determined by NFs of the first ones, hence the NF of the GC-SOA is lower when the first subsections have a better inversion. Fig. 6 shows that for low signal power a symmetric carrier distribution is obtained, while for higher power the maximum of the carrier profile moves toward the input end. Thus a decrease of the NF occurs for higher powers, provided that laser action is not turned off. This happens because the cavity gain remains constant, but the input end of the device has a higher inversion. Fig. 7 reports the forward output ASE spectra for varying input power. The output ASE decreases for increasing input power, even for input powers smaller than the saturating value, i.e., when the device still has a clamped gain. Thus the signal-ASE beating noise decreases for increasing signal, and so does the NF. The decrease of output ASE is due to the changes in the spatial carrier profile caused by the input signal. It is worth noticing that the vanishing forward ASE is added to the backward ASE. This is consistent, because for an SOA with a clamped gain the total ASE power (forward + backward) shall be approximately constant.

From Fig. 5, a small peak (0.5 dB) in the gain is observed just before saturation occurs. This effect, already reported in [7], is a consequence of the change of longitudinal carrier density profile. In fact, the gain at the lasing wavelength remains exactly constant, while at other wavelengths the gain is slightly changed, due to the dependence of the spectral material gain shape on carrier density.

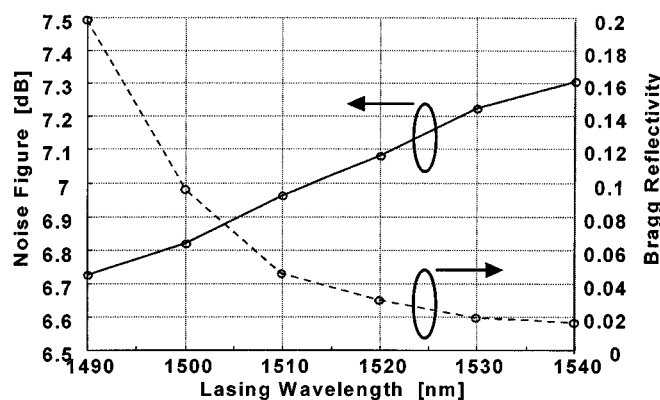


Fig. 8. NF of a GC-SOA as a function of the lasing wavelength  $\lambda_{las}$ .  $I_{act} = 100$  mA,  $\lambda_{sig} = 1550$  nm, ASE filter bandwidth = 1 nm. To maintain the same signal gain, the Bragg reflectivities  $R_1$  and  $R_2$  are varied with  $\lambda_{las}$ . Their values are reported on the right axis.

A comparison of the results of Fig. 5 with those for a conventional SOA is worthwhile. In an SOA, the increased signal power shifts the maximum of the carrier density toward the input end, but this effect is accompanied by a reduction of the overall population inversion. Thus the gain decreases and the NF increases.

We now study the dependence of GC-SOA performances on the choice of lasing wavelength. We let the lasing wavelength vary from  $\lambda_{las} = 1490$  nm to  $\lambda_{las} = 1540$  nm, while keeping the input-signal wavelength fixed at 1550 nm. The purpose of this analysis is to compare the NF of different GC-SOAs having identical other “black-box” characteristics, i.e., signal gain (18.6 dB), threshold current (28 mA), and pump current (100 mA). This is achieved by letting the Bragg grating reflectivities  $R_1$  and  $R_2$  increase as the lasing wavelength is decreased, because laser action occurs on the short-wavelength side of the gain peak. In this way, the cavity gain for the lasing mode is unity for the same injected current. Fig. 8 reports the NF as a function of lasing wavelength for  $-20$ -dBm input signal. The input power value has been chosen to keep the GC-SOA in the linear regime. The required Bragg reflectivities are also shown in Fig. 8, and

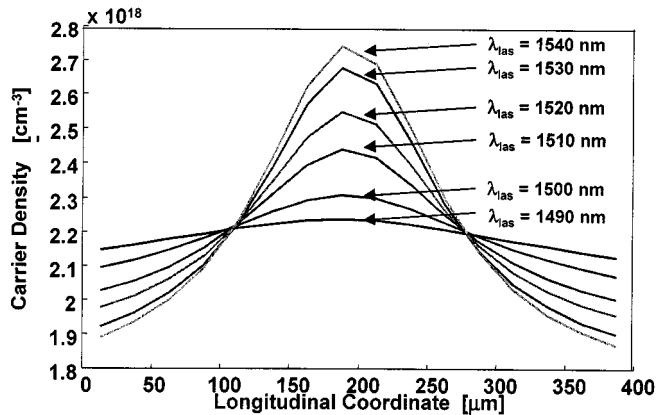


Fig. 9. Longitudinal carrier density profiles in a GC-SOA for several values of the lasing wavelength  $\lambda_{\text{las}}$  (reported on the graph).  $I_{\text{act}} = 100$  mA,  $\lambda_{\text{sig}} = 1550$  nm,  $P_{\text{in, sig}} = -20$  dBm.

range from  $R_1 = R_2 = 0.018$  for  $\lambda_{\text{las}} = 1540$  nm up to  $R_1 = R_2 = 0.2$  for  $\lambda_{\text{las}} = 1490$  nm. The NF slightly decreases for shorter lasing wavelengths, resulting in a 0.6-dB difference between the cases with  $\lambda_{\text{las}} = 1490$  nm and  $\lambda_{\text{las}} = 1540$  nm. This variation can be explained by referring to Fig. 9, that reports the longitudinal carrier densities obtained in the considered cases for  $-20$ -dBm input signal. The carrier profile is almost uniform for  $\lambda_{\text{las}} = 1490$  nm, while it has a pronounced maximum as  $\lambda_{\text{las}}$  is increased. This is due to the fact that small reflectivities generate a highly nonuniform longitudinal lasing power distribution, and a consequential pronounced depletion at the input and output ends. In turn, for the longer lasing wavelengths, the input end of the GC-SOA has a poorer inversion, and the NF is higher. The calculations show that, for all the lasing wavelengths, the same saturation output power of  $+13$  dBm is obtained. This happens despite the fact that the laser output power ranges from  $10.2$  mW for  $\lambda_{\text{las}} = 1490$  nm to  $14.8$  mW for  $\lambda_{\text{las}} = 1540$  nm, according to the spread in differential efficiency due to the changed reflectivities [10]. However, the 3-dB saturation power remains unchanged, because as soon as the laser is turned off the device behaves as a conventional SOA, and the saturation power only depends on the pump current.

The relationship between the NF and the pump current has also been analyzed, showing very little dependence. As an example, the GC-SOA with  $R_1 = R_2 = 0.03$  and with  $-30$  dBm input power has NF = 7.1 dB for  $I_{\text{act}} = 60$  mA and NF = 7.25 dB for  $I_{\text{act}} = 200$  mA. The 0.15 dB difference is caused by the slightly poorer inversion at the input end for the high pump current case [7].

All the NF results obtained here refer to a 1550-nm input signal. The calculations confirm that all trends shown above repeat themselves for different signal wavelengths, being primarily determined by the longitudinal carrier density profile within the device.

#### V. UNBALANCED GAIN-CLAMPED SOA WITH REDUCED NOISE FIGURE

In the previous section it has been demonstrated that the longitudinal profile of the carriers along the active waveguide plays an important role in determining the NF of a GC-SOA. The

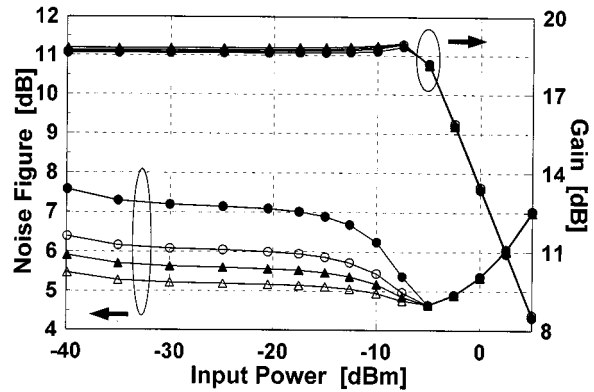


Fig. 10. Calculated gain and noise figure for balanced ( $R_1 = R_2 = 0.03$ ) and unbalanced ( $R_1 > R_2$ ) GC-SOA as a function of input signal power.  $I_{\text{act}} = 100$  mA,  $\lambda_{\text{sig}} = 1550$  nm,  $\lambda_{\text{las}} = 1520$  nm. The Bragg reflectivities  $R_1$  and  $R_2$  are chosen to keep the product  $R_1 \cdot R_2$  constant and equal to 0.0009. Solid circles:  $R_1 = R_2 = 0.03$ ; empty circles:  $R_1 = 0.06$ ,  $R_2 = 0.015$ ; solid triangles:  $R_1 = 0.09$ ,  $R_2 = 0.01$ ; empty triangles:  $R_1 = 0.18$ ,  $R_2 = 0.005$ .

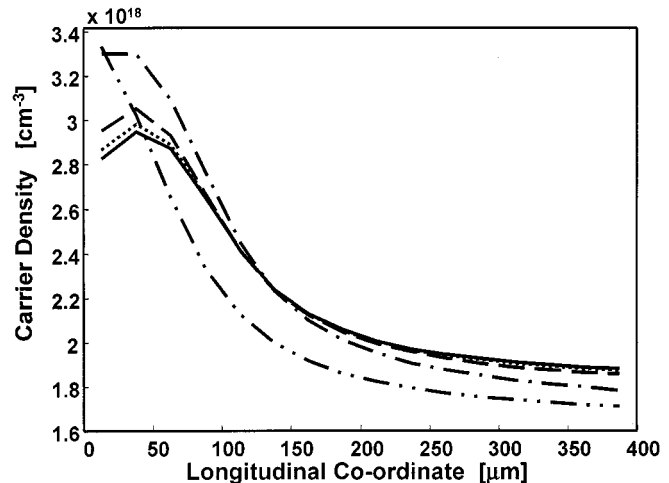


Fig. 11. Longitudinal carrier density profiles for the unbalanced GC-SOA with  $R_1 = 0.18$ ,  $R_2 = 0.005$  for several values of the input signal power.  $I_{\text{act}} = 100$  mA,  $\lambda_{\text{sig}} = 1550$  nm;  $\lambda_{\text{las}} = 1520$  nm. Solid line:  $P_{\text{in, sig}} = -40$  dBm; dotted line:  $P_{\text{in, sig}} = -17.5$  dBm; dashed line:  $P_{\text{in, sig}} = -12.5$  dBm; dash-dot line:  $P_{\text{in, sig}} = -7.5$  dBm; dash-dot-dot line:  $P_{\text{in, sig}} = 0$  dBm.

analysis of the GC-SOA by our method shows that a device with a proper carrier profile (higher inversion at the input end) would yield a lower NF for small and moderate input powers. We suggest that this can indeed be achieved by an *unbalanced* GC-SOA, i.e., a device with different Bragg reflectivities [20]. In fact, if  $R_1 > R_2$  the laser power inside the cavity is higher at the output facet, and a carrier profile with a peak closer to the input end is obtained.

In order not to vary the “black-box” characteristics of the GC-SOA other than the NF, we analyze unbalanced devices with  $R_1 > R_2$ , for which the product  $R_1 \cdot R_2$  is kept constant. Fig. 10 reports the gain and NF of the unbalanced GC-SOAs and of the balanced device as a function of input signal power. The unbalanced GC-SOAs exhibit a smaller NF with respect to the balanced device for all the input power in the linear operating range, without affecting the gain or the saturation characteristics. The unbalanced GC-SOA with  $R_1 = 0.18$ ,  $R_2 = 0.005$  allows for

an NF reduction as large as 2 dB. Also, the output forward ASE is reduced by the same amount, thus improving device cascadeability. For this device, the longitudinal carrier density as a function of input signal power is depicted in Fig. 11. The maximum of the carrier density is close to the input end also for very small signals, and almost no modification in the carrier profile is observed up to the saturation regime. Since the longitudinal carrier distribution has very small variations with input signal power, the unbalanced GC-SOA could also exhibit improved crosstalk and immunity to chirping and nonlinear effects, being particularly attractive for WDM applications. The Bragg grating reflectivity can be varied by controlling the etching depth of the DBR sections during the fabrication steps.

A discussion on the effects of the value of waveguide losses  $\alpha$  is worthwhile. All the above results are obtained for  $\alpha = 70 \text{ cm}^{-1}$ . If a value  $\alpha = 20 \text{ cm}^{-1}$  were considered, a lower carrier density would be needed to obtain laser action. The clamped gain value would be approximately the same and a 1-dB smaller NF would be achieved due to the reduced  $N_{\text{sp}}$  factor [as can be seen from (6), where the denominator is constant while the numerator decreases]. The method of unbalanced Bragg reflectivities would still be effective in further reducing the NF.

## VI. CONCLUSION

In this work, we have studied the noise figure of conventional SOAs and GC-SOAs in stationary conditions using a detailed numerical model. The model takes into account the nonuniform longitudinal carrier density by dividing the device into  $M$  subsections. It is demonstrated that at least  $M = 8$  subsections are required to obtain an accurate estimation of the SOA NF.

The model has been applied to study the NF of DBR-type GC-SOAs with respect to input power, lasing wavelength, Bragg reflectivities, and pump current. It is shown that the longitudinal profile of the carrier density determines the noise characteristics of the device, and that a high population inversion at the input end of the device is favorable for a low NF. Longer lasing wavelengths give slightly higher NFs, as well as higher pump currents. A new method for the reduction of GC-SOA noise figure has been proposed, based on unbalanced Bragg reflectors. NF improvement as large as 2 dB has been devised.

## ACKNOWLEDGMENT

The authors wish to thank Prof. S. Donati of University of Pavia, Pavia, Italy, for his useful suggestions and encouragement during this work. They also wish to thank D. Campi, C. Coriasso, and M. Vallone of CSELT, Torino, Italy, for interesting discussions.

## REFERENCES

- [1] W. van Berlo, M. Janson, L. Lundgren, A. C. Mórner, J. Terlecki, M. Gustavsson, P. Granstrand, and P. Svensson, "Polarization-insensitive, monolithic 4'4 InGaAsP-InP laser amplifier gate switch matrix," *IEEE Photon. Technol. Lett.*, vol. 7, pp. 1291–1293, Nov. 1995.
- [2] F. Dorgeuille, W. Grieshaber, F. Pommereau, C. Porcheron, F. Gaborit, I. Guillemot, J. Y. Emery, and M. Renaud, "First array of 8 CG-SOA gates for large-scale WDM space switches," in *European Conf. Optical Communications '98*, Madrid, Spain, Sept. 1998, pp. 255–256.

- [3] L. F. Tiemeijer, P. J. A. Thijs, T. v. Dongen, J. J. M. Binsma, E. J. Jansen, and H. R. J. R. van Helleputte, "Reduced intermodulation distortion in 1300 nm gain-clamped MQW laser amplifiers," *IEEE Photon. Technol. Lett.*, vol. 7, pp. 284–286, 1995.
- [4] C. Holtmann, P.-A. Besse, T. Brenner, and H. Melchior, "Polarization independent bulk active region semiconductor optical amplifier for 1.3  $\mu\text{m}$  wavelengths," *IEEE Photon. Technol. Lett.*, vol. 8, pp. 343–345, Mar. 1996.
- [5] K. Obermann, I. Koltchanov, K. Petermann, S. Diez, R. Ludwig, and H. G. Weber, "Noise analysis of frequency converters utilizing semiconductor-laser amplifiers," *IEEE J. Quantum Electron.*, vol. 33, pp. 81–88, Jan. 1997.
- [6] J. Sun, G. Morthier, and R. Baets, "Numerical and theoretical study of the crosstalk in gain clamped semiconductor optical amplifiers," *IEEE J. Select. Topics Quantum Electron.*, vol. 3, pp. 1162–1167, Nov./Dec. 1997.
- [7] J. L. Plummekeers, M.-A. Dupertuis, T. Hessler, P. E. Selbmann, S. Haacke, and B. Deveaud, "Longitudinal spatial hole burning and associated nonlinear gain in gain-clamped semiconductor optical amplifiers," *IEEE J. Quantum Electron.*, vol. 34, pp. 879–886, 1998.
- [8] D. Wolfson, S. L. Danielsen, C. Joergensen, B. Mikkelsen, and K. E. Stubkjaer, "Detailed theoretical investigation of the input power dynamic range for gain-clamped semiconductor optical amplifier gates at 10 Gb/s," *IEEE Photon. Technol. Lett.*, vol. 10, pp. 1241–1243, Sept. 1998.
- [9] M. Shtaf and G. Eisenstein, "Experimental study of the statistical properties of nonlinearly amplified signals in semiconductor optical amplifiers," *IEEE Photon. Technol. Lett.*, vol. 9, pp. 904–906, July 1997.
- [10] G. P. Agrawal and N. K. Dutta, *Long-Wavelength Semiconductor Lasers*. New York: Van Nostrand Reinhold, 1986.
- [11] T. Kamiya, "Radiative and nonradiative recombinations in semiconductors," in *Semiconductor Lasers and Photonic Integrated Circuits*, Y. Suetatsu and A. R. Adams, Eds. London: Chapman & Hall, 1994.
- [12] O. Svelto, *Principles of Lasers*. New York: Plenum, 1989.
- [13] L. Thylén, "Amplified spontaneous emission and gain characteristics of Fabry-Perot and traveling wave type semiconductor laser amplifiers," *IEEE J. Quantum Electron.*, vol. 24, pp. 1532–1537, 1988.
- [14] M. J. Adams, J. V. Collins, and I. D. Henning, "Analysis of semiconductor laser optical amplifiers," *Inst. Elec. Eng. Proc.—Part J.*, vol. 132, no. 1, pp. 58–63, 1985.
- [15] G. Giuliani, "Semiclassical particle-like description of optical amplifier noise," *Opt. and Quantum Electron.*, vol. 31, pp. 367–376, 1999.
- [16] S. Donati and G. Giuliani, "Noise in an optical amplifier: Formulation of a new semiclassical model," *IEEE J. Quantum Electron.*, vol. 33, pp. 1481–1488, Sept. 1997.
- [17] M. Norgia, G. Giuliani, and S. Donati, "Noise evolution along optically amplified links in presence of nonlinear parametric gain," *J. Lightwave Technol.*, vol. 17, pp. 1750–1757, Oct. 1999.
- [18] E. Desurvire, *Erbium-Doped Fiber Amplifiers—Principle and Applications*. New York: Wiley, 1994.
- [19] T. Mukai and Y. Yamamoto, "Noise in AlGaAs semiconductor laser amplifier," *IEEE J. Quantum Electron.*, vol. 18, pp. 564–575, 1982.
- [20] G. Giuliani, D. D'Alessandro, and S. Donati, "Analysis of gain-clamped SOA's with reduced noise figure," in *European Conf. Optical Communications '99*, vol. 1, Nice, France, Sept. 1999, pp. 358–359.

**Guido Giuliani** (M'99) was born in Milan, Italy, in 1969. He received the degree (with honors) in electronic engineering and the Ph.D. degree in electronics and computer science from Università di Pavia, Pavia, Italy, in 1993 and 1997, respectively.

He is now a Postdoctoral Researcher at the Dipartimento di Elettronica, Università di Pavia. His main research interests are diode laser feedback interferometry, optical amplifier noise, semiconductor optical amplifiers, and electro-optical gyroscopes.

**Davide D'Alessandro** (S'00) was born in Milan, Italy, in 1975. He received the degree (with honors) in electronic engineering from Università di Pavia, Pavia, Italy, in 1998. He is currently working towards the Ph.D. degree in electronics and computer science at the University of Pavia, in the Electrooptics group.

His research interests are noise in semiconductor optical amplifiers, backscattering measurements in optical fibers, and interferometry.